Improving positioning performance of positive position feedback scheme with delay compensation

Paul, Ager; Küçükdemiral, Ibrahim; Bevan, Geraint

Published in:
2023 9th International Conference on Control, Decision and Information Technologies (CoDIT)

DOI:
10.1109/CoDIT58514.2023.10284322

Publication date:
2023

Document Version
Author accepted manuscript

Improving Positioning Performance of Positive Position Feedback Scheme with Delay Compensation

Ager Paul[1], Ibrahim Küçükdemiral[1] and Geraint Bevan[1]

***Abstract*— Piezoelectric stack-actuated serial kinematic nanopositioning stages are widely utilized in nanopositioning applications but are plagued by challenges such as hysteresis, creep, and mechanical resonance, which degrade system performance. Closed-loop control, particularly positive position feedback (PPF) control, has shown the potential in mitigating these issues and achieving robust nanopositioning. This study focuses on evaluating the performance of PPF control in nanopositioning, specifically considering closed-loop stability. To address the inherent time delay effects in piezoelectric stack actuated nanopositioners, a PPF controller is designed to achieve stable and robust operation. The impact of time delay in flexure nanopositioners is analyzed through simulation-based frequency response analysis, revealing the relationship between the period of the peak-to-peak of the error signal simulation and the performance of the PPF controller. The study demonstrates that a gain of 7.84 dB is required for the PPF controller with delay to become unstable. The design methodology incorporates second-order Padé approximations, allowing the system to be represented by eight poles. Among these poles, five are determined by the controller's parameter design, while the remaining three are influenced by the system's delay. To ensure desirable system behavior, the five designed poles are positioned closer to the imaginary axis compared to the three poles introduced by the delay. The analysis identifies an upper limit of $\tau = 342\mu s$ for the permissible delay, beyond which the poles introduced by the delay surpass some of the designed poles' proximity to the imaginary axis. This situation undermines the dominance of the designed poles and compromises system performance. The findings emphasize the critical relationship between the error signal simulation and the performance of the PPF controller. This study provides valuable insights for improving controller design and ensuring stable nanopositioning systems. The results also highlight the importance of addressing time delay effects in flexure nanopositioners to achieve robust and reliable performance.**

Key Words

Nanopositioning stage, Positive Position Feedback (PPF), vibration control, time delay, tracking

I. Introduction

Nanopositioning systems play a crucial role in various applications where precise nanoscale motion is required [1]. These applications include surface inspection [2], [3], scanning probe microscopy [4], Nanofabrication [5] and imaging of fast biological and physical processes [6]. However, the performance of nanopositioning stages can be affected by issues such as harmonic excitation, resonance, hysteresis, and drift [7]. To overcome these challenges and minimize positioning errors, feedback and/or feedforward control systems are employed. Characterizing the performance of nanopositioning systems is essential but often lacks clear and consistent guidelines. While terms like accuracy, precision, and resolution are commonly used, their evaluation methods vary [8]. Precision is typically assessed by measuring steady-state positioning noise, accuracy is determined by the variability of positioning error across the system's range, and resolution refers to the smallest achievable motion indicated by peak-peak positioning noise [9], and RMS tracking error is also commonly used as a performance measure [10].

Damping control techniques are employed to address mechanical resonance limitations by artificially increasing the damping ratio of the system [11]. By increasing the damping ratio, the feedback gain and closed-loop bandwidth can be proportionally enhanced when using an integral controller. Several successful damping control techniques have been proposed in the literature, including Integral Resonant Control [12], Positive Position Feedback [13], [14], Resonant control [15], shunt control [16] and polynomial based control [17]. Polynomial-based controllers have primarily been used to damp systems where a lightly-damped resonant mode at a low frequency dominates the dynamics, and higher modes are sufficiently distant from the first mode. These systems include flexible manipulators [18], disc-drive actuators [19], high-density memory storage devices [20], nanopositioning platforms, and more [17]. However, positive Position feedback (PPF) controllers demonstrate robustness in the face of parameter uncertainties. The Positive Position Feedback (PPF) controller is a damping control technique used to reduce vibrations in flexible beams and structures. Its purpose is to achieve shorter settling times and attenuate vibrations. This control technique can also be extended to mitigate vibrations in aircraft wings, making it applicable in the aerospace industry. Apart from controlling structural vibrations, the PPF controller can also be utilized for managing sound waves, leveraging its resonant control capabilities. While considerable attention has been given to the identification, modeling, and control of the mechanical structure and piezoelectric actuators in these systems, the dynamics of the piezoelectric drive circuit, displacement sensor, and electronic control circuit are often overlooked due to the assumption that their dynamics are significantly faster than the mechanical components. However, these components can introduce time delays that become significant across the broad bandwidth of the nanopositioning system [21],

*This work was not supported by any organization

[1]The authors are with the Department of Applied Science, School of Computing, Engineering and Built Environment, Glasgow Caledonian University, 70 Cowcaddens Rd, G4 0BA, Glasgow, UK. Emails: pager200@caledonian.ac.uk, iku1@gcu.ac.uk, geraint.bevan@gcu.ac.uk.

[22]. The presence and impact of such delays were initially observed in a previous work, where the delay introduced by the finite clock speeds of the signal conditioning electronic equipment associated with displacement sensors was quantified. The stability conditions of the positive position feedback (PPF) scheme was extended to account for the effects of the delay using Padé approximation. Comparing the Padé methods, it has been observed that higher-order schemes offer greater efficiency for achieving high accuracy [23]. In fact, fourth-order Padé methods have been employed for solving the two-dimensional sGE in previous studies [24]. These Padé methods incorporate the nonlinearity treatment from the finite difference scheme developed by Perring and Skyrme [25]. This paper introduces the concept of PPF with delay, and it is found that there exists a linear relationship between the sampling time and the introduced delay. The dynamical model of the system is designed to incorporate the identified delay, and the methodology for designing the PPF control scheme is extended to address this delay. This extension enables the derivation of analytically exact expressions, facilitating the study of closed-loop system stability to determine the maximum permissible delay before encountering instability. Conventional delay compensation techniques like the Smith predictor [26] and direct inversion of plant dynamics, are not applicable to piezoelectric nanopositioners. The presence of an infinite number of unmodeled vibration modes hinders the use of the Smith predictor, and the direct inversion of plant dynamics is infeasible due to the time delay introducing non-minimum phase (NMP) zeros, which would lead to unstable poles. Therefore, it is necessary to explore the quantification and compensation of delay in the system to address these challenges.

II. Organization

The following is how the paper is structured: Section 2 presents background theory for second-order resonant systems. A model of one axis of a piezo-actuated nanopositioning platform is developed in this section. Section 3 presents the full parametric analysis of the PPF damping controller scheme, including delay compensation. Section 4 presents closed-loop results for the controller implemented, as well as an analysis of the results. Section 5 brings the paper to a close.

III. Background Theory

The system's dynamics are modeled as a mass-spring-damper system with an equation of motion.

$$m\ddot{x}(t) + b\dot{x}(t) + kx(t) = F(t) \tag{1}$$

where m is the platform's mass, b is the damping coefficient of the flexures, k is the spring stiffness of the flexures, and F is the force applied by the actuator. Taking the Laplace transform of the equation of motion, the transfer function measured from the applied force, F, to the displacement, x, is

$$G(s) = \frac{X}{F} = \frac{1}{ms^2 + bs + k} = \frac{\frac{1}{m}}{s^2 + \frac{b}{m}s + \frac{k}{m}} \tag{2}$$

In addition, the natural frequency $\omega_n = \sqrt{\frac{k}{m}}$ A dominant lightly-damped resonant mode is evident in the frequency response of a typical nanopositioner measured from output displacement of one axis to input command signal to the same axis [10]. However, the dynamics beyond the first mode fade quickly and can (and usually are) ignored; despite the fact that the useful model of a nanopositioner axis reduces to a lightly-damped second-order transfer function with an additional feed-through to compensate for the truncation of high-frequency response data [18]. This can be represented using equation (2) above after substituting standard variables by

$$G(s) = \frac{\gamma^2}{s^2 + 2\zeta\omega_n s + \omega^2 n} + d_f$$

where $\zeta, \omega_n, d_f$are the damping ratio, undamped natural frequency, and the feedback through the term. Also $\gamma^2 = dc_{gain} \times \omega^2 n$ The design and application of positive position feedback (PPF) to dampen the dominant resonant mode of such systems are well documented. The controller used is positive position feedback as shown in fig. 1 and its generic structure is presented below

$$Cd_{\text{PPF}} = \frac{\Gamma_1}{s^2 + 2\zeta_c\omega_c s + \omega_c^2} \tag{3}$$

And the tracking controller, C_t, is an integrator given by

$$C_t(s) = \frac{k_t}{s} \tag{4}$$

IV. Controller synthesis for positive position feedback

Using the plant model given by (3) and the controller transfer function given by (4), the overall transfer function of the closed-loop system can be written as

$$\frac{Y(s)}{R(s)} = \frac{{G_{\text{cl}}}^{num}}{{G_{\text{cl}}}^{den}}$$

Where

$$\begin{gathered}
{G_{\text{cl}}}^{num}(s) = K_t\Gamma^2(s^2 + 2\zeta_c\omega_c s + \omega_c^2) \\
{G_{\text{cl}}}^{den}(s) = s^5 + (2\zeta\omega_n + 2\zeta_c\omega_c)s^4 \\
+(2\zeta\omega_n 2\zeta_c\omega_c + \omega_n^2 + \omega_c^2)s^3 \\
+(2\zeta\omega_n\omega_c^2 + 2\zeta_c\omega_c\omega_n^2 + K_t\Gamma^2)s^2 \\
+(\omega_n^2\omega_c^2 - \gamma^2\Gamma_1 + k_t\gamma^2 2\zeta_c\omega_c)s \\
+(k_t\gamma^2\omega_c^2)
\end{gathered} \tag{5}$$

${G_{\text{cl}}}^{dem}(s)$ can be expressed as

$$P(s) = s^5 + k_4 s^4 + k_3 s^3 + k_2 s^2 + k_1 s + K_0 \tag{6}$$

Where the resulting coefficients of k_n are

$$k_4 = 2\zeta\omega_n + 2\zeta_c\omega_c$$

$$k_3 = 2\zeta\omega_n 2\zeta_c\omega_c + \omega_n^2 + \omega_c^2)$$

$$k_2 = 2\zeta\omega_n + 2\zeta_c\omega_c\gamma_n^2 + k_t\gamma^2$$

$$k_1 = \omega_n^2\omega_c^2 - \gamma^2\Gamma_1 + k_t\gamma^2 2\zeta_c\omega_c$$

$$k_0 = k_t\gamma^2\omega_c^2 \tag{7}$$

Equation (7) can be expressed as follows

$$2\zeta_c\omega_c = k_4 - 2\zeta\omega_n$$

$$\omega_c^2 = k_3 - \omega_n^2 - 2\zeta\omega_n 2\zeta_c\omega_c$$

$$K_t = \frac{k_0}{(\gamma^2\omega_c^2)}$$

$$k_2 = 2\zeta\omega_n + 2\zeta_c\omega_c\gamma_n^2 + k_t\gamma^2$$

$$\Gamma_1 = \frac{(\omega_n^2\omega_c^2 + 2\zeta_c\omega_c\gamma^2 k_t - k_1)}{\gamma^2} \tag{8}$$

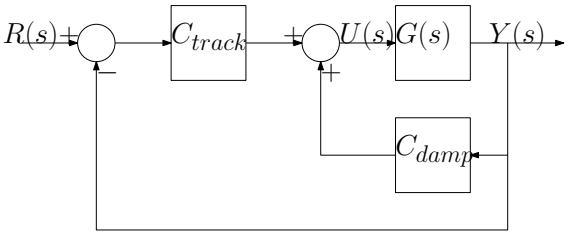

Fig. 1. Block diagram of the closed-loop control scheme with tracking

V. PPF Control scheme with delay compensation

The theoretical model of the platform is modified to include the effects of delay leading to the expression shown below:

$$G(s) = \frac{\gamma^2 e^{-\tau s}}{s^2 + 2\zeta\omega_n s + \omega_n^2} \tag{9}$$

Where τ is the value of the time delay in the system. Considering equation (13) the closed-loop transfer function is written as follows:

$$\frac{Y(s)}{R(s)} = \frac{{Z_{\text{cl}}}^{num}}{{Z_{\text{cl}}}^{den}} \tag{10}$$

$${Z_{\text{cl}}}^{num}(s) = \gamma^2(K_t s^2 + 2sk_t\omega_c\gamma + k_t\omega_c^2)e^{-\tau s}$$

$${Z_{\text{cl}}}^{den}(s) = s^5 + (2\zeta\omega_n + 2\gamma\omega_c)s^4$$

$$+(2\zeta\omega_n 2\gamma\omega_c + \omega_n^2 + \omega_c^2)s^3$$

$$+(2\zeta\omega_n\omega_c^2 + 2\zeta_c\omega_c\omega_n^2 + k_t\gamma^2)s^2$$

$$+(\omega_n^2\omega_c^2 + (k_t\gamma^2 2zeta_c\omega_c - \gamma^2\Gamma_1)e^{-\tau s})s$$

$$+k_t\gamma^2\omega_c^2 e^{-\tau s} \tag{11}$$

${Z_{\text{cl}}}^{num}(s)$ can be expressed as

$$P(s) = s^5 + k_4 s^4 + k_3 s^3 + k_2 s^2 + k_1 s + k_0 \tag{12}$$

Where the resulting coefficients of k_n from the characteristic equation P(s) are

$$k_4 = 2\zeta\omega_n + 2\gamma\omega_c$$

$$K_3 = 2\zeta\omega_n 2\gamma\omega_c + \omega_n^2 + \omega_c^2$$

$$k_2 = 2\zeta\omega_n\omega_c^2 + 2\zeta_c\omega_c\omega_n^2 + k_t\gamma^2$$

$$k_1 = \omega_n^2\omega_c^2 + (k_t\gamma^2 2zeta_c\omega_c - \gamma^2\Gamma_1)e^{-\tau s}$$

$$k_0 = k_t\gamma^2\omega_c^2 e^{-\tau s} \tag{13}$$

Equation (14) can be solved by leading to the following:

$$2\gamma\omega_c = k_4 - 2\zeta\omega_n$$

$$\omega_c^2 = k_3 - \omega_n^2 - 2\zeta\omega_n 2\gamma\omega_c$$

$$k_t = \frac{k_0}{\gamma^2\omega_c^2 e^{-\tau s}}$$

$$k_2 = 2\zeta\omega_n\omega_c^2 + 2\zeta_c\omega_c\omega_n^2 + k_t\gamma^2$$

$$\Gamma_1 = -\frac{k_1 - \omega_n^2\omega_c^2 - (k_t\gamma^2 2\zeta_c\omega_c e^{-\tau s})}{\gamma^2 e^{-\tau s}} \tag{14}$$

VI. System Modeling

The frequency response of the nanopositioner's x-axis was recorded. A lightly-damped resonance mode at 713Hz is visible on the platform axis. Using the platform parameters, a second-order transfer function that accurately captures the dominant resonant dynamics of this axis was obtained. A feedthrough term of 0.029 was added to account for the truncation of the higher-frequency dynamics. The transfer function with the feedthrough term that results is given in (16).

$$G(s) = \frac{9.888 \times 10^6}{s^2 + 116.5s + 2.007 \times 10^7} + 0.029 \tag{15}$$

This control design is based on the $G(s)$ transfer function model. FRF was obtained several times for different sampling times ranging from 50 to 200 μs in increments of 20 μs s in order to identify the dependence of the delay on the sampling time. The following system model was identified using the six measurements

$$G(s) = \frac{9.888 \times 10^6 e^{-\tau s}}{s^2 + 116.5s + 2.007 \times 10^7} \tag{16}$$

Where the delay τ is given as

$$\tau = \frac{1}{2}T_s + 90 \times 10^{-6} \tag{17}$$

Where T_s is the sampling time. Both the delay τ and the sampling time are expressed in seconds.

It can be observed that the resonance frequency of the plant is 713Hz and there is a near-linear relationship between the sampling period and the delay introduced in the system. The chosen frequency range captures the first three resonance modes of the platform and shows the effect of the uncertainty of the system. The presence of delay can be observed in the phase response of figure (3). Although three resonance modes have been identified in the measured FRF, only the first is considered in the design of the PPF control scheme as the first mode is dominant. In order to identify the dependence of the delay on the sampling time, several FRF were obtained for different sampling times ranging from 30 to 90 μs in increments of 20 μs. The delay of the system is due to two different phenomena: The fixed delay of 90 μs determined by the latency system (50 μs) and the mechanical design of the nanopositioner (40 μs), secondly, there is a delay proportional to half the sampling time as predicted by Janschek, 2011; Philips and Nagle, 1995.

VII. Simulation Results

This section presents the simulation results obtained by applying the traditional PPF and PPF with delay compensation. It is observed that in the PPF control scheme with delay, the maximum delay admissible in the plant before encountering instability is above that shown by PPF control scheme without delay and allows the use of slower sampling rates and inexpensive equipment without significant loss in performance. However, failing to account for the delay present in the nanopositioning system can result in performance degradation and instability issues in the closed-loop control. The PPF controller is used in this article to demonstrate these issues. The controller parameters are derived using [27] approach, the PPF and the tracking controller results in the following;

$$C_{\text{damp}\,PPF} = \frac{3.258e^{07}}{s^2 + 8017s + 4.548e^{07}} \tag{18}$$

$$C_{\text{track}}(s) = \frac{1550}{s} \tag{19}$$

Figure 3 depicts the magnitude response of the simulated closed-loop system and the measured magnitude response for various sampling times, despite the fact that each sampling time is associated with a different delay determined by (17). The response does not achieve a flat band response and as the sampling time is increased with the associated delay, the system's performance deteriorates. It can also be seen that the presence of delay causes the five designed poles to be displaced from their original location, causing them to no longer conform to the Butterworth pattern and thus preventing the obtained flat magnitude response.

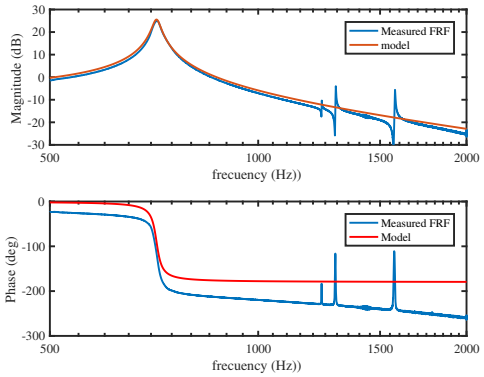

Fig. 2. FRF of the platform and the second-order model without delay measured from the output to the output displacement.

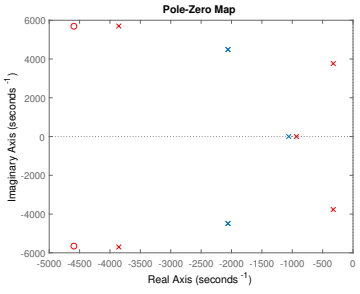

Fig. 3. The pole-zero map of the PPF scheme

VIII. Analysis/Discussion of the Results

The PPF control scheme with delay demonstrates superior performance compared to the PPF scheme without delay. Moreover, the PPF with delay can be applied to a wide range of systems with varying delays, resulting in improved

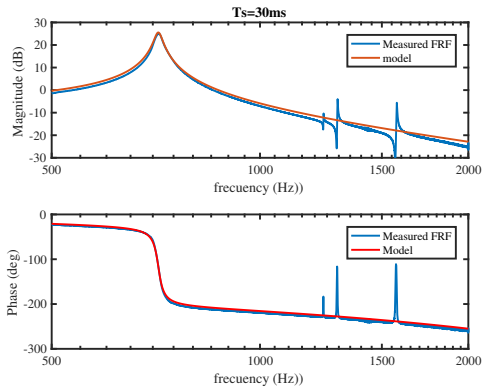

Fig. 4. Magnitude and phase response of nanopositioning platform for 30ms sampling rate

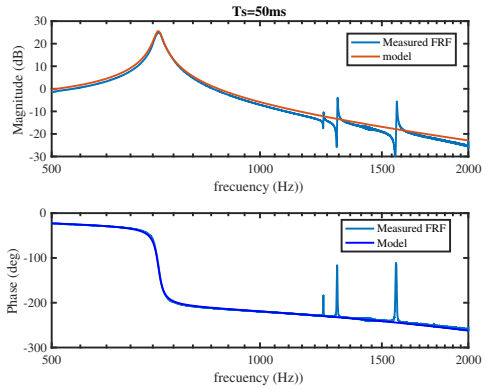

Fig. 5. Magnitude and phase response of nanopositioning platform for 50ms sampling rate

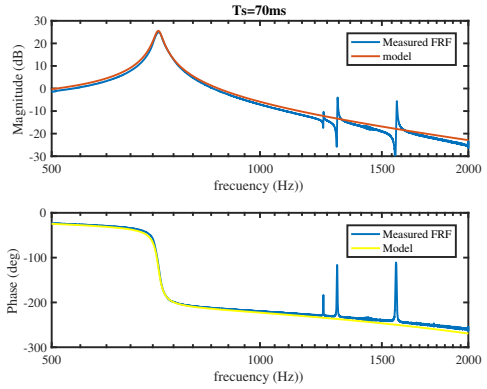

Fig. 6. Magnitude and phase response of nanopositioning platform for 70ms sampling rate.

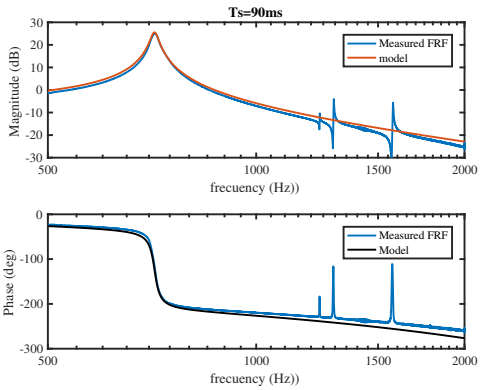

Fig. 7. Magnitude and phase response of nanopositioning platform for 90ms sampling rate

performance in the presence of uncertainties in the system delay. The Padé approximation [28] method is employed to estimate the effect of delay, offering advantages such as computational simplicity and accurate fitting of time moments. Poles introduced by Padé approximations in the closed-loop control system are utilized to assess whether the designed five poles in the closed-loop are dominant over the poles introduced by the delay. To ensure the dominance of the designed poles, a second-order Padé approximation of the delay is utilized to determine the pole placement in the closed-loop system. The Padé approximation [29]: For $n > 1$. The $[n, n]$ Padé approximant is given by

$$e^{-\tau s} = \frac{P(-s)}{P(s)} \tag{20}$$

Where

$$P(s) = \sum_{k=0}^{n} \binom{n}{k} \frac{k!(2n-k)!}{2n!} s^k \tag{21}$$

By substituting the Padé approximations into the transfer function's exponential terms in the closed-loop system, the characteristic equation is formed with eight poles. Among these poles, five are determined by the controller's parameter design, while the remaining three are introduced by the second-order Padé approximations to represent the system delay. [30]. Figure 4 illustrates the closed-loop frequency response of the damped system, meeting the performance specifications as the controller adequately dampens the system.

The design objective of the PPF control scheme with delay compensation is to ensure that the five designed poles along a circle with a radius of ω_n are dominant over the delay-induced poles. These designed poles are considered dominant because their proximity to the imaginary axis is greater than the poles introduced by the delay. It is observed that the delay introduced an infinite number of closed-loop poles while the second-order Padé approximations are only used to compute a finite number of closed-loop system roots. The dominance of five designed poles is checked over a finite number of poles because any meaningful pole introduced by

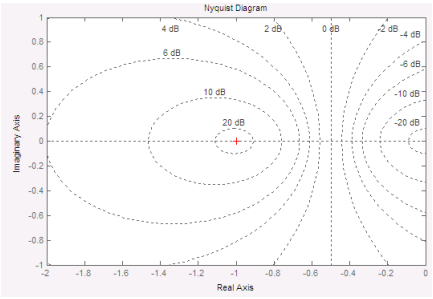

Fig. 8. The Nyquist plot of the open loop system

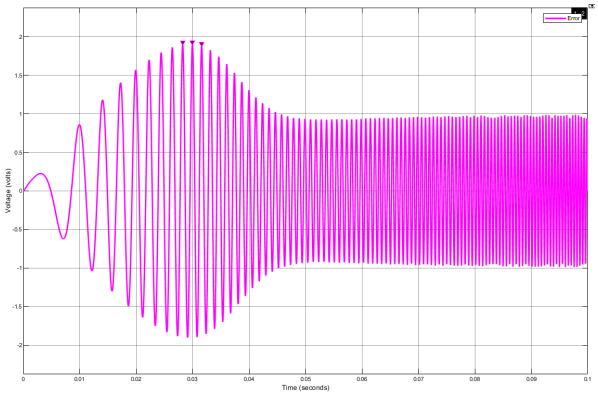

Fig. 9. Error of the PPF scheme

the delay would be located further from the imaginary axis than those introduced by the Padé approximations. Figure 6 illustrates the position of the closed-loop poles for the entire system when the delay is increased in the range $\tau = [0.800CL1 or 0.700CL2]\mu s$. As the delay is increased, the three poles introduced by the Padé approximations move closer to the imaginary axis. Hence, an upper limit of the maximum permissible delay, $\tau = 342\mu s$is suggested. Any delay value exceeding $\tau = 342\mu s$ would place the poles introduced by the Padé approximations closer to the imaginary axis than some of the designed poles. The impact of the poles introduced by the delay becomes significant in systems where the delay exceeds the maximum applicable range. Figure 8 presents a polar plot of the open-loop gain. It is observed that point -1 was encircled clockwise, indicating system stability with a magnitude of 1 and an angle of -180 degrees. This implies that the point is positioned one unit away from the origin on the negative real axis. The analysis of Figure 9 provides valuable insights into the performance of the PPF Controller by examining the difference between the chirp signal and the plant output. Notably, the error signal exhibits a peak value of 1.914 within a duration of 0.289s. Further characterization of the error signal reveals a Peak-to-Peak value of 3.828 and an RMS value of 0.8283. Additionally, the overshoot is measured at 6.656% with an amplitude of 1.876V. Throughout the simulation, it is observed that the difference in error bounds initially increases at the onset, spanning the first 0.289s, and subsequently decreases thereafter. This trend indicates that the controller's

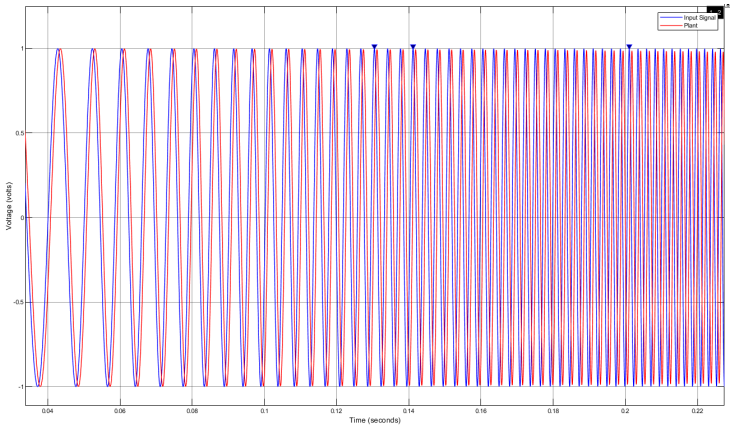

Fig. 10. Reference tracking of the PPF controller

performance begins to deteriorate following the Peak-to-Peak time of 0.289s. To provide a quantitative measure of this degradation, the ratio of the Error Peak-to-Peak time to the total simulation time, expressed as a percentage, that is

$$\frac{Error(peak-to-peak)_{\text{time}}}{t_{\text{end}}} \times 100$$

can be used. In this particular case, the degradation time for the controller amounted to 28.8% of the simulation time, as depicted in Figure 10.

The data presented highlights the importance of monitoring the degradation of reference tracking in relation to the simulation time. Understanding the temporal dynamics of controller performance is crucial for assessing its overall effectiveness and identifying potential areas for improvement.

TABLE I

Simulated Results of Traditional PPF and PPF with Delay

Controller	3dB (Hz)	Gain Margin	Phase Margin
PPF(trad.)	705.09	3.55dB	180deg
PPF(delay)	698.9	7.84dB	69.2deg

IX. Conclusion

This article presents a technique for adjusting the parameters of the PPF control method, enabling flexible positioning of the dominant closed-loop poles in nanopositioning systems that experience time delay. The study compared the performance of the traditional PPF control and the PPF control with delay, revealing that the latter outperformed the former. The results indicate that the introduced delay in the nanopositioner can be determined by the sampling rate employed and should not be disregarded due to its noticeable impact. Additionally, the traditional PPF control's performance significantly worsened with increased sampling time. On the other hand, the PPF controller with delay exhibited an optimal response across a wide range of acceptable sampling times and delays. These findings demonstrate the potential to utilize PPF with slower sampling rates, thereby reducing the equipment cost for electronic control systems. Future research endeavors will be dedicated to enhancing the

performance of the controller beyond the current limitation of 28% of the simulation time. This will involve investigating and implementing novel strategies to mitigate the observed degradation and optimize the controller's functionality. Furthermore, it is imperative to validate the efficacy of the improved controller on a diverse range of electromechanical systems. By subjecting the controller to different system characteristics and operating conditions, its robustness and adaptability can be thoroughly evaluated. This empirical testing will provide valuable insights into the controller's generalizability and ascertain its effectiveness across various practical scenarios. The objective of these future investigations is to advance the state-of-the-art in controller design and address the existing limitations, thereby facilitating the broader application of the controller in real-world electromechanical systems. The outcomes of such endeavors will contribute to the development of more reliable and efficient control strategies, ultimately enhancing the performance and stability of diverse electromechanical systems.

REFERENCES

[1] A. H. Slocum, *Precision machine design*. Society of Manufacturing Engineers, 1992.

[2] G. Borionetti, A. Bazzali, and R. Orizio, "Atomic force microscopy: a powerful tool for surface defect and morphology inspection in semiconductor industry," *The European Physical Journal Applied Physics*, vol. 27, no. 1-3, pp. 101–106, 2004.

[3] S. Devasia, E. Eleftheriou, and S. R. Moheimani, "A survey of control issues in nanopositioning," *IEEE Transactions on Control Systems Technology*, vol. 15, no. 5, pp. 802–823, 2007.

[4] M. J. Brukman and D. A. Bonnell, "Probing physical properties at the nanoscale," *Physics Today*, 2008.

[5] J. Vicary and M. Miles, "Pushing the boundaries of local oxidation nanolithography: Short timescales and high speeds," *Ultramicroscopy*, vol. 108, no. 10, pp. 1120–1123, 2008.

[6] M. Kobayashi, K. Sumitomo, and K. Torimitsu, "Real-time imaging of dna–streptavidin complex formation in solution using a high-speed atomic force microscope," *Ultramicroscopy*, vol. 107, no. 2, pp. 184–190, 2007.

[7] J. Mondal and S. Chatterjee, "Controlling self-excited vibration of a nonlinear resonant velocity feedback with time-delay," *International Journal of Non-Linear Mechanics*, vol. 131, May 2021.

[8] N. B. Hubbard and L. L. Howell, "Design and characterization of a dual-stage, thermally actuated nanopositioner," *Journal of Micromechanics and Microengineering*, vol. 15, no. 8, p. 1482, 2005.

[9] W. O'Brien, "Long-range motion with nanometer precision," *Photonics Spectra*, vol. 39, no. 6, pp. 80–81, 2005.

[10] S. S. Aphale, B. Bhikkaji, and S. Moheimani, "Minimizing scanning errors in piezoelectric stack-actuated nanopositioning platforms— nova. the university of newcastle's digital repository," 2008.

[11] A. J. Fleming and K. K. Leang, "An experimental comparison of pi, inversion, and damping control for high performance nanopositioning," in *American Control Conference (ACC), 2013*. IEEE, 2013, pp. 6027–6032.

[12] S. S. Aphale, A. J. Fleming, and S. R. Moheimani, "Integral resonant control of collocated smart structures," *Smart Materials and Structures*, vol. 16, no. 2, p. 439, 2007.

[13] J. Fanson and T. K. Caughey, "Positive position feedback control for large space structures," *AIAA Journal*, vol. 28, no. 4, pp. 717–724, 1990.

[14] M. Eissa, M. Karnel, N. Saeed, W. EI-Ganaini, and H. EI-Gohary, "Time-delayed positive position and velocity feedback controller to suppress the lateral vibrations in nonlinear jeffcott-rotor system," *Manufiya Journal of Electronic Engineering Research (MJEER)*, July 2018.

[15] A. Sebastian, A. Pantazi, S. Moheimani, H. Pozidis, and E. Eleftheriou, "A self servo writing scheme for a mems storage device with sub-nanometer precision— nova. the university of newcastle's digital repository," 2008.

[16] A. J. Fleming and S. Moheimani, "Sensorless vibration suppression and scan compensation for piezoelectric tube nanopositioners— nova. the university of newcastle's digital repository," 2006.

[17] S. S. Aphale, B. Bhikkaji, and S. R. Moheimani, "Minimizing scanning errors in piezoelectric stack-actuated nanopositioning platforms," *IEEE Transactions on Nanotechnology*, vol. 7, no. 1, pp. 79–90, 2008.

[18] I. Mahmood, S. Moheimani, and B. Bhikkaji, "Precise tip positioning of a flexible manipulator using resonant control— nova. the university of newcastle's digital repository," 2007.

[19] G. Cherubini, C. C. Chung, W. C. Messner, and S. R. Moheimani, "Control methods in data-storage systems," *IEEE Transactions on Control Systems Technology*, vol. 20, no. 2, pp. 296–322, 2012.

[20] B. Bhikkaji, M. Ratnam, A. J. Fleming, and S. R. Moheimani, "High-performance control of piezoelectric tube scanners," *IEEE Transactions on Control Systems Technology*, vol. 15, no. 5, pp. 853–866, 2007.

[21] C.-X. Li, Y. Ding, G.-Y. Gu, and L.-M. Zhu, "Damping control of piezo-actuated nanopositioning stages with recursive delayed position feedback," *IEEE Transactions on Mechatronics*, vol. 22, pp. 855–864, April 2017.

[22] S. Roy, I. N. Kar, J. Lee, N. G. Tsagarakis, and D. G. Caldwell, "Adaptive robust control of a class of el systems with parametric variations artificially delayed input and position feedback," *IEEE Transactions on Control Systems Technology*, pp. 1063–6536, 2017.

[23] D. Duncan, "Sympletic finite difference approximations of the nonlinear klein-gordon equation," *Numer Anal*, vol. 34(5), pp. 1742–60. doi: 10.1137/ S0 036 142 993 243 106 ., 1997.

[24] Y. Luo, X. Li, and C. Guo, "Fourth-order compact and energy conservative scheme for solving nonlinear klein-gordon equation. numer meth part differ equ," *International Journal of Non-Linear Mechanics*, vol. 33(4), p. 1283–304. doi: 10.1002/num.22143, 2016.

[25] J. Perring and T. Skyrme, "A model unified field equation," *Nucl Phys*, vol. 31, pp. 550–5. doi: 10.1016/0029– 5582(62)90 774– 5 ., 1962.

[26] S. Li, J. Li, K. Zhang, and Y. Mo, "Output prediction based active disturbance rejection control approach and its application in structural vibration," in *Control Conference (CCC), 2014 33rd Chinese*. IEEE, 2014, pp. 3614–3619.

[27] D. Russell, A. J. Fleming, and S. S. Aphale, "Simultaneous optimization of damping and tracking controller parameters via selective pole placement for enhanced positioning bandwidth of nanopositioners," *America control conference (ACC)*, no. 7, pp. 2184–2189, 2014.

[28] Y. Shamash, "Order reduction of linear systems by padé approximation methods," 1973.

[29] J. R. Partington, "Some frequency-domain approaches to the model reduction of delay systems," *Annual Reviews in Control*, vol. 28, no. 1, pp. 65–73, 2004.

[30] A. San-Millan, D. Russell, V. Feliu, and S. S. Aphale, "A modified positive velocity and position feedback scheme with delay compensation for improved nanopositioning performance," *Smart Materials and Structures*, vol. 24, no. 7, p. 075021, 2015.